

Article

The Analyses of Land Use and Prevention in High-Density Main Urban Areas under the Constraint of Karst Ground Subsidence: Study of Wuhan City, China

Lin Gao ¹ , Yan Shi ², Yang Qiu ¹, Chuanming Ma ^{1,*} and Aiguo Zhou ¹

¹ School of Environmental Studies, China University of Geosciences, No. 388 Lumo Road, Wuhan 430074, China; glin@cug.edu.cn (L.G.)

² TianDiTu Center, Yunnan Provincial Mapping Institute, No. 223 Xichang Road, Kunming 650031, China

* Correspondence: machuanming@cug.edu.cn; Tel.: +027-67883157 (ext. 430074)

Abstract: The development and utilization of land in the main urban area have significantly impacted the stability of the regional geological environment through various means, such as increased load and subway construction, primarily manifested as rock and soil mass deformation leading to geological hazards. Therefore, it is worth exploring how to reduce the occurrence of karst ground subsidence (KGS) through reasonable land development and control measures in the main urban areas with large-scale developments of buried karst formations. This study focuses on the main urban area of Wuhan City. An evaluation model for KGS was constructed using the analytic hierarchy process (AHP) and comprehensive index evaluation method by analyzing the geological conditions that affect KGS. The susceptibility zoning of KGS was obtained with GIS spatial analysis technology. The results show that the susceptible areas can be divided into extreme, high, medium, and weak susceptibility, accounting for 4.93%, 15.30%, 33.21%, and 46.56%, respectively, which are consistent with the distribution density of past KSGs. Furthermore, by selecting the subway construction as a human activity type, it indirectly discusses the influence of land development intensity on KGS. The results show that past KSGs are mainly concentrated in areas with high engineering construction density and significant land development intensity. Based on the above, strategies for regional land development and prevention and control of KGSs are proposed.

Keywords: main urban area; land development and utilization; buried karst ground subsidence; susceptibility assessment



Citation: Gao, L.; Shi, Y.; Qiu, Y.; Ma, C.; Zhou, A. The Analyses of Land Use and Prevention in High-Density Main Urban Areas under the Constraint of Karst Ground Subsidence: Study of Wuhan City, China. *ISPRS Int. J. Geo-Inf.* **2023**, *12*, 425. <https://doi.org/10.3390/ijgi12100425>

Academic Editors: Jiangfeng She, Jun Zhu, Min Yang and Wolfgang Kainz

Received: 8 August 2023

Revised: 17 September 2023

Accepted: 11 October 2023

Published: 16 October 2023



Copyright: © 2023 by the authors. Licensee MDPI, Basel, Switzerland. This article is an open access article distributed under the terms and conditions of the Creative Commons Attribution (CC BY) license (<https://creativecommons.org/licenses/by/4.0/>).

1. Introduction

Carbonate rock formations are widely present in the ice-free continental areas of the Earth and provide water resources for 20% to 30% of the world's population [1–3]. The carbonate rock formations in mountainous areas are directly exposed to the surface, resulting in prominent karst landforms [4]. These areas often accompany mining and tourism activities like Guilin Karst Landscapes [5]. The carbonate rock formations in the plain are usually covered by Quaternary sediments, making it challenging to determine carbonate rocks' distribution range accurately. This can adversely affect engineering construction, such as highways and high-rise buildings [6]. Karst ground subsidence (KGS) usually occurs in carbonate rock beneath the Quaternary sediments [7,8]. The main reason is that carbonate rock generally has cavities and voids, and channels are connected to the covered sediment. Under natural and human factors, Quaternary sediments leak along karst channels, resulting in KGS [9].

To prevent the hazards caused by KGS, extensive research has been conducted on karst subsidence development's geological and environmental conditions. Siska et al. (2016) and YongYao and ShuLin (2018) found that the underground water flow conditions, lithology of bedrock, voids, and karst caves in the bedrock, as well as changes in water and gas pressure

within the pores, are significant influencing factors [10,11]. Kaufmann and Quinif 2002 and Zhao et al. 2018 investigated how to identify the distribution characteristics of KGS from the ground and conducted case studies using techniques such as ground remote sensing, ground penetrating radar, seismic imaging, etc. [12,13]. Several studies [14–18] have investigated the triggering mechanisms of KGS, using various analytical methods such as microgravity measurement, logistic regression analysis, and the information value method or experimental simulation, and found that factors such as unstable surface sediments, land development and utilization, poor surface drainage, and high surface slope can affect the occurrence of KGS. However, the above research primarily focuses on large areas and wide plain suburbs, emphasizing the KGS phenomenon's causal mechanisms and statistical laws. Some scholars mainly study the susceptibility to KGS in the construction sites of major linear projects. A few scholars utilize historical, geophysical, and geological methods to analyze karst environments to prevent urban development in hazardous areas [19–21]. However, there is still a lack of analysis from both the perspective of geological, environmental conditions and the intensity of large-scale engineering construction activities regarding the restrictive effect of karst ground collapse on land use in central urban areas (small-scale areas with high-intensity human activities). Similarly, insufficient research identifies factors causing different regional karst ground collapses and proposes targeted control measures for land development and utilization in central urban areas [22–24].

As a developing country still undergoing continuous and rapid urbanization, China's urban area continues to expand, and the population density in cities is rapidly increasing. The rapid modernization of cities has led to changes in land use patterns in the main urban areas, mainly manifested by inefficient land use patterns in the early stages of urban development [25]. Local governments have carried out large-scale demolition and reconstruction of central urban areas to cope with population growth and economic development, along with many engineering constructions such as subways and high-rise residential buildings [26]. Wuhan is the capital city of Hubei Province, a rapidly developing city and the most populous city in central China. It is an important transportation hub in the region, located in the eastern part of the Jiangnan Plain, where the Yangtze River and its longest tributary, the Han River, converge [27–29]. In 2021, the main urban area, including seven districts, had a population of about 7 million residents with an average population density of 7974 people per square kilometer (Figure 1). This exceeds Greater London's population density of 5726 people per square kilometer and is similar to Tokyo's population density of 7846 people per square kilometer, but it is lower than New York City's population density of 11,002 people per square kilometer [30–32]. Wuhan's extremely high population density is accompanied by economic development and the improvement of the regional urbanization level, leading to continuous urban renewal and large-scale urban construction [33–35].

The subway network is a pioneer in urban development, providing convenient commuting conditions that expand people's living range. As a result, it could change the land use value or utilization methods of areas surrounding the subway lines. This often leads to demolishing, rebuilding buildings, and developing and utilizing vacant land [36–38]. The demolition and reconstruction of buildings often involve transforming old, low-rise residential houses into newly commercial office buildings, high-rise apartments, etc., which increases the ground load and imposes higher requirements on the carrying capacity of the regional geological environment [39–41]. During the abovementioned construction process, various construction methods were employed, such as drilling, pile foundation reinforcement, excavation of foundation pits, and dewatering. These methods have led to changes in the primary geological conditions of the project area. While developing and utilizing vacant land, activities such as filling in sinkhole lakes and excavating soil can directly change the regional geo-environmental conditions by affecting groundwater systems' discharge and replenishment conditions and causing changes in the thickness of overlying bedrock layers. Therefore, during the construction process of the subway, not only will the construction process directly affect the stability of the rock formations in the subway construction area,

but it will also indirectly lead to changes in land use patterns around the railway line and consequently alter regional geo-environmental conditions [18,42]. The renewal and construction of the central urban area are mainly centered around subway lines. The building or planning of subway lines can reflect the strength of regional development [43,44].

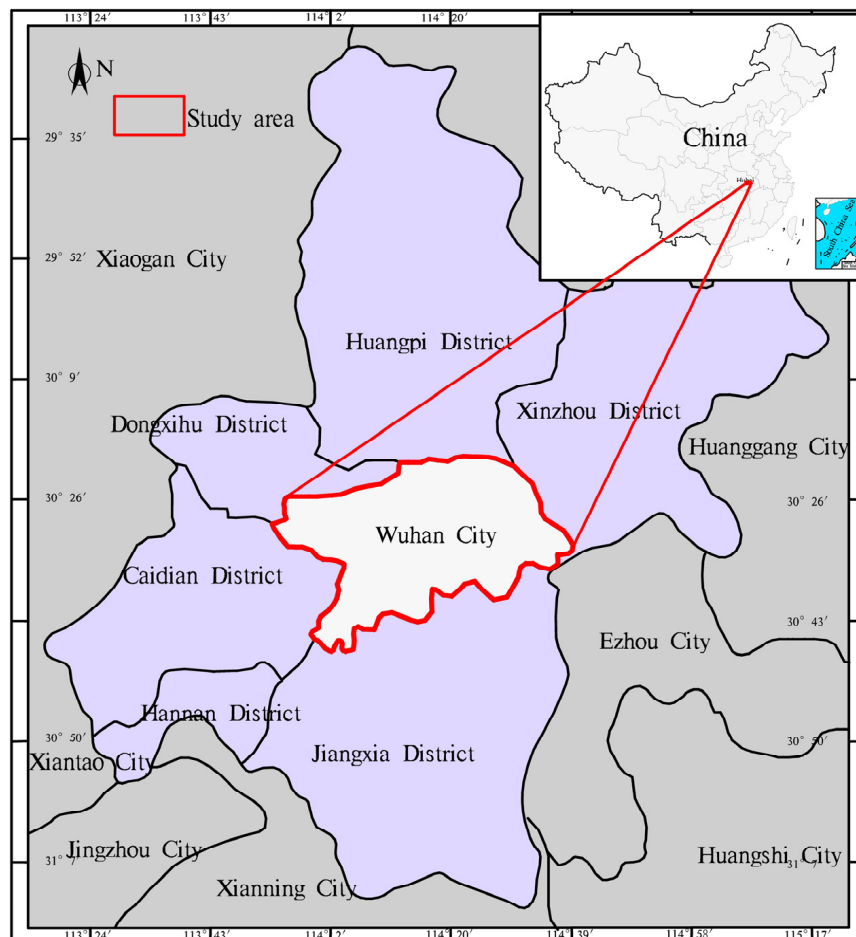


Figure 1. Location and scope of the study area.

Three soluble carbonate rock belts are distributed in the main urban area of Wuhan, running approximately east–west. The width of these belts generally ranges from 0.8 to 6.8 km. Due to tectonic movements, some parts of the belts have undergone folding, and only a tiny amount is exposed, while the majority remains concealed beneath Quaternary sediments. These belts represent typical buried karst formations in southern China [45]. In the context of the widespread distribution of buried karst formations, the large-scale urban construction and land development in Wuhan have been restricted by geological hazards such as KGS. Therefore, this study selected the main urban area of Wuhan City as the study area, which has dense subway lines and buried carbonate rock formations. By analyzing the ways and influencing factors of high-intensity human activities on the susceptibility of buried KGS within a small range, corresponding land development control measures and suggestions are proposed based on the evaluation results in the central urban area.

2. Karst Development Conditions

Wuhan has a subtropical, humid monsoon climate with an average annual precipitation of 1140–1265 mm. The rainfall is concentrated from April to August. It belongs to a part of the Yangtze River through depression and has sub-platform characteristics. The strata comprise the Silurian–Quaternary (S–Q) group, among which the Quaternary distribution in this area is the widest, accounting for about 85% of the total area. The central

zone is dominated by plains in the landform, with low mountains and hills alternating with plains [46,47]. The fractures are well developed, with several running almost through the entire area from north to south. The groundwater types are divided into three categories according to aquifers' lithology and occurrence conditions: sedimentary pore water, carbonate rock fissure water, and clastic rock fissure water. The distribution of the aquifer is shown in Figure 2 [48].

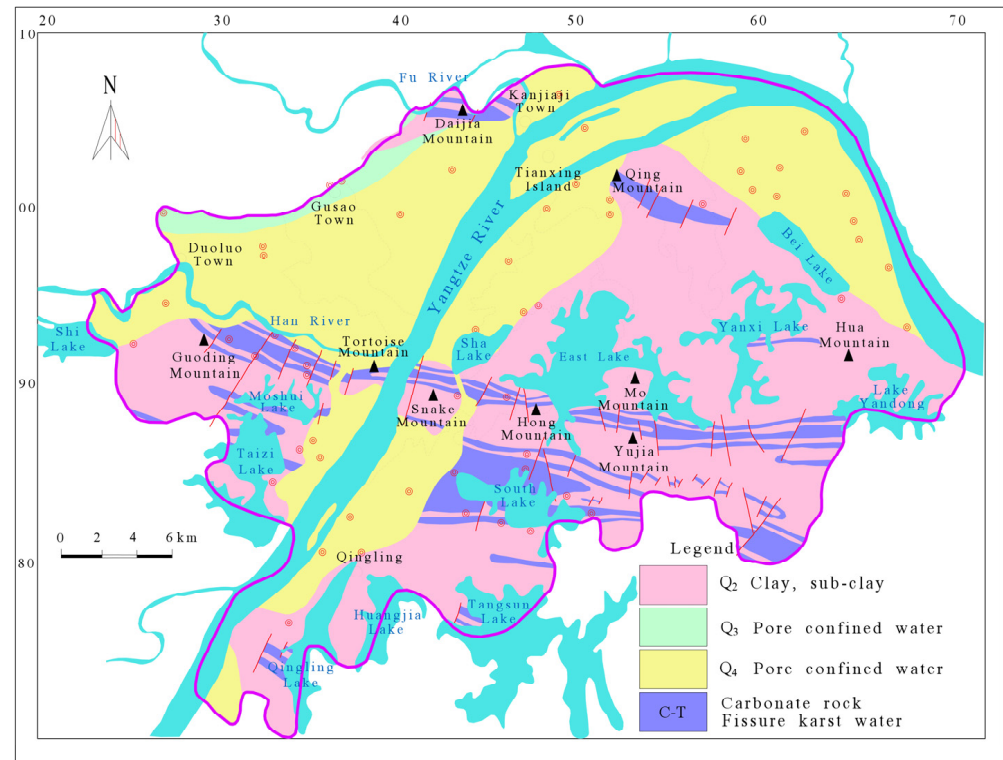


Figure 2. Hydrogeological map of the study area.

The development degree of carbonate rock karst and the distribution of ground subsidence caused by karst can be seen in Figure 2 of the study area. There are three nearly east–west buried carbonate rock belts distributed in the area.

A. Daijia Mountain–Qing Mountain

Located in the northernmost part, most of this area is dominated by dolomite and siliceous dolomite, with a small amount of siliceous limestone mixed in. The CaO/MgO ratio is low, and the SiO₂ content is high in its chemical composition. The main rock-forming minerals are dolomite, pyrite, quartz, and calcite. It is relatively difficult to dissolve and has no apparent dissolution phenomenon. But in some local areas, the geological structure has a significant impact, with well-developed karstification, such as near the Tianxingzhou Yangtze River Bridge.

B. Guoding Mountain–Guishan–Yujia Mountain

This belt can be further divided into three small belts. The middle belt mainly comprises T_{1-2j}, T_{1d}, P_{1q}, and P_{1g} dolomitic limestone and argillaceous limestone, while the two sides mainly comprise C_{2h} limestone and dolomite. It is covered by Q₂ sticky soil with a thickness ranging from 12 to 51.

C. Moshui Lake–South Lake

This belt can be further divided into three small belts. The middle belt is relatively wide, with small and slender belts on both sides, located in the core area of the Xinglong–Baoxi complex inverted anticline. It mainly comprises dolomite, limestone,

mudstone, and other rocks. Some areas contain non-soluble rocks, such as siliceous rock, shale, and claystone, with a localized presence of red sandstone. Except for the area near Wuchang Railway Station, which is covered by Quaternary old clay, the rest is covered by loose sediments such as alluvium and lake deposits.

There are 11 subway lines already built in the research area, with four under construction and three planned for future development. The construction process of subway lines directly involves engineering activities such as underground excavation, drilling, and drainage; it also indirectly affects changes in land use around the lines and places higher demands on the regional geological environment carrying capacity. In recent years, ground subsidence caused by karst has occurred more frequently in the study area. It is the most significant geological hazard threatening people's lives and property safety. This restricts the development and utilization of land in the main urban area. In the study area, KGS mainly manifests as the subsidence of Quaternary loose deposits. According to official records and research data, there have been 27 incidents of karst subsidence in the study area. From the perspective of geological structure analysis, the occurrence of KGS is mainly located near fault zones, and its probability is inversely proportional to the distance from the Yangtze River. Based on drilling data interpretation, dissolution is evident near fractured zones with an average limestone dissolution rate of 27%. From the perspective of the distribution of soluble lava formations, KGSs mainly occur in the Triassic Daye Formation and Permian Qixia Formation limestone, all of which belong to buried karst subsidence [42]. From the coverage structure and thickness perspective, 23 occurrences belong to the binary structure of "upper adhesive lower sand", and 4 occurrences belong to structures with three or more layers. The number of occurrences for soil layer thicknesses of 20–30 m and 30–40 m is 18 and 9 times, respectively.

According to the geological conditions, triggering mechanisms, and relevant monitoring data of karst subsidence in the main urban area [49], the presence of karst cavities, a certain thickness of the loose cover layer, and groundwater dynamics are the basic conditions for KGS. This study analyzes the susceptibility of KGS from three basic conditions: karst conditions (KCs), overburden conditions (OCs), and hydrodynamic conditions (HCs). Based on ignoring factors that have little impact on basic conditions, we further decompose basic conditions into six influencing factors: bedrock lithology (KC_{BL}), degree of karstification (KC_{DK}), thickness of overburden OC_T , lithology and structure of overburden OC_{LS} , distance between groundwater level and bedrock HC_{DLB} , and variation in groundwater level HC_{VL} [17,50–53].

3. Method

Many complex and intertwined factors contribute to the subsidence of karst ground, presenting a complex nonlinear dynamic characteristic among various influencing factors. However, there is also an apparent correlation and classification [23]. The traditional qualitative evaluation method cannot comprehensively reflect the multi-factor effects of KGS. The analytic hierarchy process (AHP) is a multi-objective decision-making analysis method that combines qualitative and quantitative methods, which avoids determining weights directly by evaluators and reduces the subjective factors affecting the evaluation [54–56]. It is suitable for analyzing the interrelated and interdependent complex problems of factors such as those in KGS susceptibility assessment, enabling quantitative evaluation of KGS.

3.1. Evaluation Model

A multi-factor discrimination model for evaluating ground subsidence in karst areas is established based on the basic conditions and influencing factors' analysis and selected evaluation methods (Figure 3).

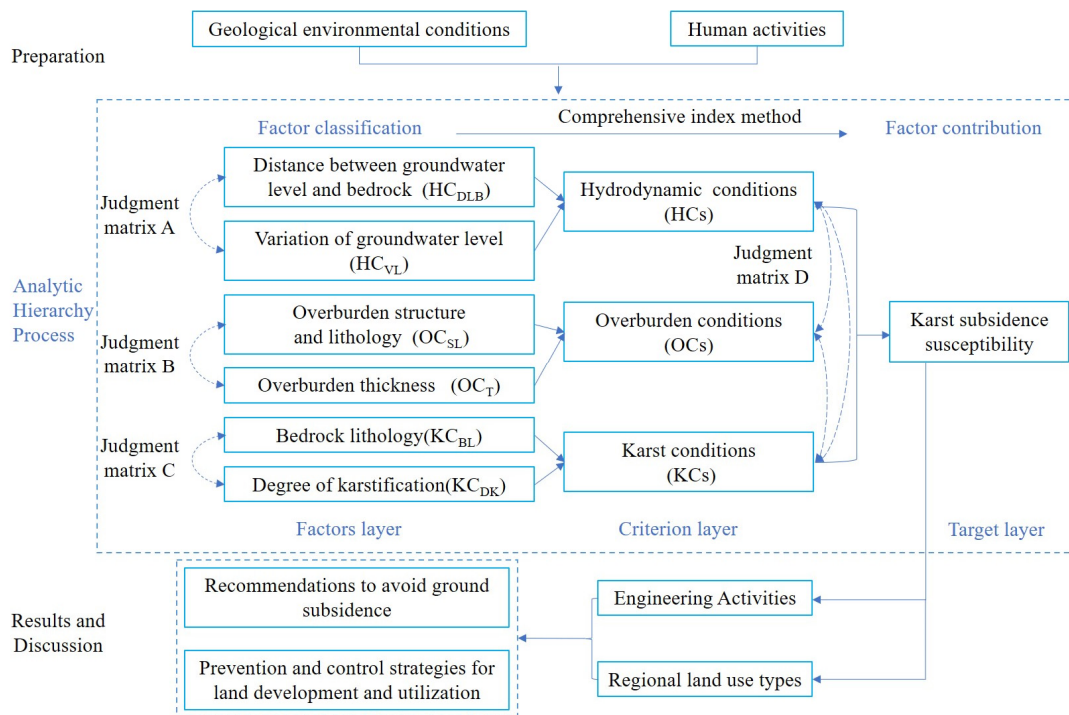


Figure 3. The flowchart of this study.

According to the corresponding status of influencing factors in different regions, their contribution degree to ground subsidence in karst areas is analyzed and divided into levels using the 1–9 scale method. A weighted average comprehensive index model is applied to evaluate the susceptibility of karst subsidence [56,57]

$$PI_i = \sum_{j=1}^m w'_{ij} \cdot P_{ij} \quad (1)$$

where PI_i represents the comprehensive score of the i -th evaluation unit and P_{ij} represents the comprehensive score of the i -th evaluation unit.

The flowchart in Figure 3 outlines the process for assessing KGS.

Firstly, analyze the contribution and quantify the grading of six influencing factors to their respective basic conditions based on their specific situations in different areas.

Secondly, construct a judgment matrix according to the relative importance by expert knowledge of influencing factors under the same basic condition, obtain eigenvectors, conduct consistency checks and normalization processing, and obtain weights for the six influencing factors on basic conditions.

Thirdly, repeat the steps above to determine the contribution level and importance of three basic conditions to KGS.

Fourthly, the contribution level of influencing factors to KGS can be obtained by multiplying each pair of basic conditions and influence factor weights, and a KGS susceptibility zoning map can be obtained using the comprehensive index method to superimpose influence factors based on MAPGIS.

Finally, it examines the limitations and preventive measures for high-density urban land development caused by karst coverage, considering engineering construction activities like subway construction, regional land use status and planning, and susceptibility analysis of KGS.

3.2. Factors Affecting Karst Ground Subsidence

This section mainly introduces the evaluation factors of KGS. It explains in detail the impact of these factors on the development and occurrence of KGS. There are three main indicators and six factors, as shown in Table 1. The following is a detailed explanation.

Table 1. The evaluation factor level classification criteria of karst ground subsidence.

Indicators	Factors	Levels				Data Sources
		Weak	Medium	High	Extreme	
Karst conditions	Bedrock lithology	S, D, N, K-E	T	P	C	National Geological Archive Data Center http://dc.ngac.org.cn/ ; accessed on 7 September 2020
Overburden conditions	Degree of karstification	-	Fissure developed	Few caves, fissure developed	Caves developed	Wuhan Center of China Geological Survey https://zk.cgsi.cn/ accessed on 7 September 2020
	Thickness Lithology and Structure	>30 m Single clay layer	30–20 m Clay–Sand ratio>1	20–10 m Clay–Sand ratio<1	<10 m Single sand layer	
Hydrodynamic conditions	Pore water level to bedrock distance	-	30–15 m	-	<15 m	Geogical Environmental Center of Hubei https://geocloud.hubgs.com/metadata/ accessed on 7 September 2020
	Ground level variation	<1 m	1–3 m	3–5 m	>5 m	

Karst conditions (KCs)

The KGS areas of Wuhan City mostly appear in subsidence pits and other point-like forms. The subsidence pits are distributed linearly in space, while there are also cases where they appear concentrated in the same area. The distribution characteristics of the subsidence events show a pattern of points, lines, and areas strongly correlated with the lithology of bedrock and the degree of karst development [58,59].

Bedrock lithology (KC_{BL})

The highest karst erosion rate in the research area is found in the thick layer of limestone from the Carboniferous–Permian Chuanshan Formation–Huanglong Formation (C), where local caves are developed. The second highest rate is found in the thick layer of limestone in the Permian Qixia Formation (P). The karst erosion rate could be better for the Triassic Daye Formation mudstone (T), with only a few dissolution fissures. There is no karst development in the Silurian (S), Devonian (D), Cretaceous and Lower Tertiary (K-E), and Upper Tertiary (N) clastic rock bedrock (Figure 4a).

Degree of karstification (KC_{DK})

According to the collected data from 279 borehole rock cores, the underground karst features in the area were statistically analyzed. The results showed that the main karst forms are caves and dissolution fissures. Influenced by crustal uplift and subsidence, there is a specific stratification vertically, with caves and crevices mainly distributed above –45 m elevation. In the A. belt, karst development is more significant within the elevation range of –50~5 m; the B. Belt has overall well-developed karst features, with the most significant development at elevations of 10~15 m and –5~–10 m; and the C. Belt has relatively developed karst features at elevations of 0~5 m and –25~–40 m. The height of caves is generally between 0.1 and 6 m, with longitudinal string-like cave phenomena present. The filling rate of caves is low, and they are usually filled with clay or gravel. Karst development can be classified into four categories: no karst development; well-developed fissures; few caves but well-developed fissures; and relatively developed caves and crevices (Figure 4b).

Overburden conditions (OCs)

The subsidence process of Quaternary loose deposits can be divided into two stages. In the first stage, sandy soil leaks and subsidence occur due to changes in groundwater dynamic conditions. Sandy soil produces vertical leakage at the rock–soil interface, forming funnel-shaped loose bodies. In the second stage, the cohesive soil cover layer becomes unstable. When the funnel-shaped open body of sandy soil spreads to the cohesive soil cover layer, the bottom of the coherent soil cover layer loses support force. It causes central

subsidence in the cohesive soil funnel. A subsidence pit is formed when it is further affected by additional loads or insufficient buoyancy pressure caused by human activities. The effect of this subsidence process is closely related to the thickness of cohesive soils, and its occurrence location is closely associated with overlying rock structure types; a single-structure covering layer may only experience one or both stages, while dual-structure covering layers will experience both stages simultaneously [60].

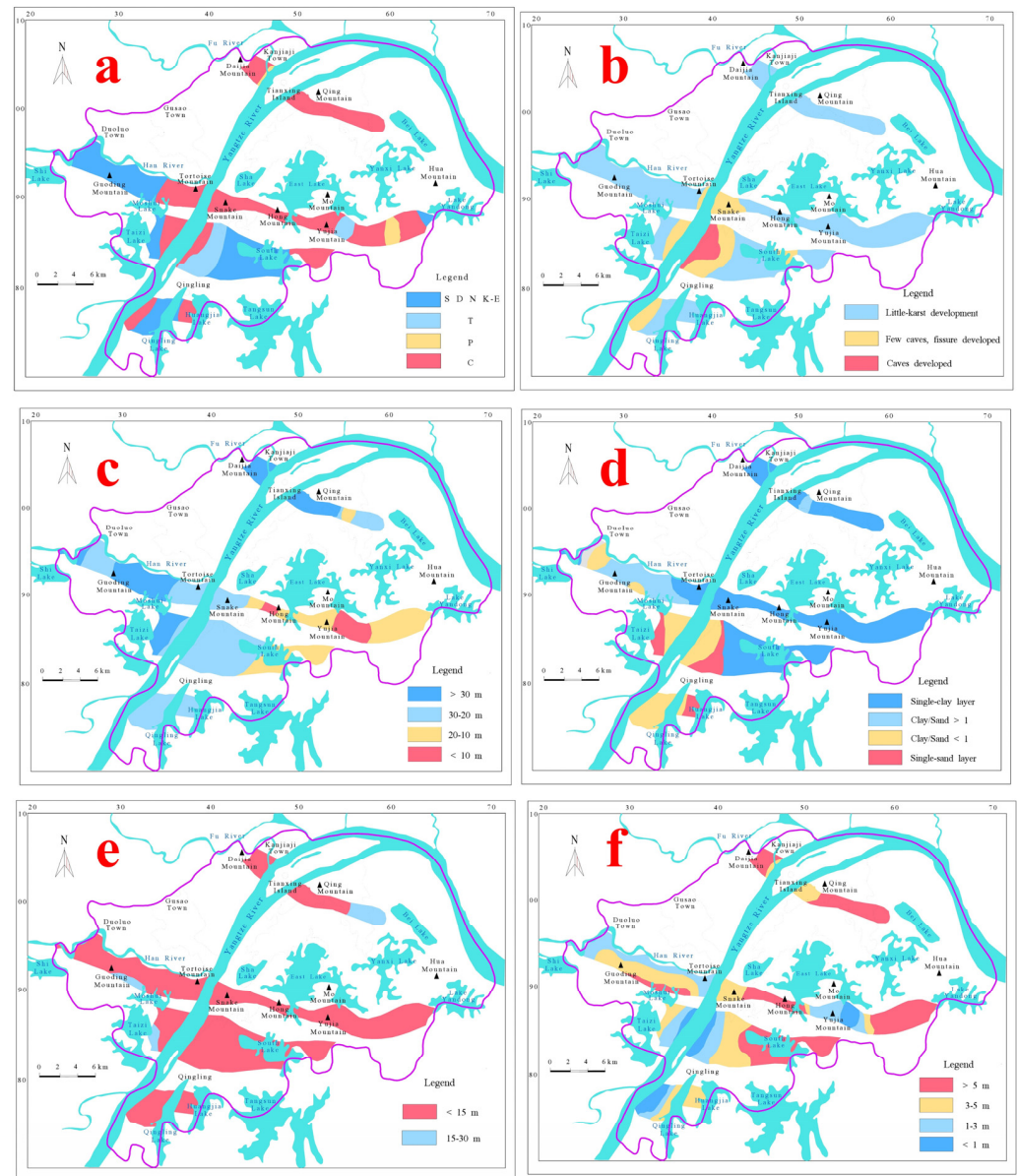


Figure 4. Single-factor zoning map. (a): Bedrock lithology; (b): degree of karstification; (c): overburden thickness; (d): overburden structure and lithology; (e): distance between groundwater level and bedrock; (f): variation in groundwater level.

Overburden thickness (OC_T)

Based on the collected drilling data, the thickness of the Quaternary cover layer was statistically analyzed for each borehole. The thickness data of the Quaternary cover layer in the study area were obtained by Kriging interpolation. Previous studies have shown an inverse relationship between the thickness of the Quaternary cover layer and the probability of karst subsidence, i.e., a thicker cover layer indicates a lower probability of karst subsidence. According to statistics, most karst subsidence occurs in areas where the

thickness of the covering layer is less than 10 m, with areas with less than 5 m having the highest density and the most significant amount of subsidence. The subsidence decreases significantly in areas where covering layers are between 10 and 30 m thick, and almost no subsidence occurs in areas with more than 30 m thick covering layers. In this study, based on the geological properties of Quaternary sediments and the analysis and summary of available data on past occurrences of subsidence, influencing factors were divided into four levels: >30 m, 30–20 m, 20–10 m, and <10 m (Figure 4c).

Overburden structure and lithology (OC_{SL})

According to the geological survey and drilling data, the Quaternary cover layer structure in the study area can be divided into single-layer and binary structures. The single-layer structure is generally plastic cohesive soil with sufficient consolidation and strong cohesion, which is not prone to subsidence. The binary structure has two situations: the first type with the upper layer made of plastic or hard plastic clay, and the lower layer composed of gravelly sub-soil, with a clay–sand ratio greater than 1. In this case, the probability of subsidence is relatively tiny; the second situation is that the upper layer is plastic clay, and the lower layer consists of sand–gravel or sandy soil with a clay–sand ratio of less than 1. Due to direct contact between sand layers and carbonate rocks, karst fissures or cavities cause sand–gravel or sandy soil leakage, leading to a high probability of the karst subsidence phenomenon. In this study, the material composition and structural aspects of cover layers are classified as follows: single-clay layer; clay–sand ratio greater than 1; clay–sand ratio less than 1; single-layer sandy soil (Figure 4d).

Hydrodynamic conditions (HCs)

The influence of groundwater dynamic conditions on karst subsidence mainly manifests in the erosion effect of pore water on saturated sand. The overlying loose layer pore water head is higher than karst water. It has pressure-bearing properties, which are conducive to carrying loose sand particles into karst fissures and cavities for migration, resulting in infiltration erosion [9]. At the same time, the fluctuation range of the bedrock groundwater level directly affects the change in the groundwater hydraulic gradient, exacerbating the erosion effect of the cover sediment. According to the monitoring data, the hydraulic head difference between the pore and karst water in the study area ranges from −1.14 to 15.93 under natural conditions, and their water levels change synchronously. According to physical model experiments, critical hydraulic gradients for permeability deformation in sand layers were 0.31~0.73, while destructive critical hydraulic gradients were 0.675~4.49 [49,58]. Therefore, the distance between the groundwater level and the bedrock surface and the groundwater level fluctuation are chosen as influencing factors to analyze the impact of groundwater level on karstification.

Distance between groundwater level and bedrock (HC_{DLB})

Analyzing existing karst subsidence events, the characterization of the distance between the groundwater level and bedrock surface is obtained by calculating the distance between the average annual elevation of the pore water level and the elevation of the bedrock surface. The reason is that if the groundwater level in the pore fluctuates near the top surface of the bedrock, it will quickly increase the erosive force on the sand layer and cause subsidence. According to statistics on karst subsidence events in the study area, those with a distance of less than 15m are prone to induce subsidence. In comparison, those greater than 15 m are relatively stable and do not easily trigger subsidence. The distance between pore water levels and bedrock in the study area is divided into two groups, 15–30 m and <15 m (Figure 4e).

Variation in groundwater level (HC_{VL})

The change in groundwater level can be expressed by its variation. The greater the deviation of groundwater level, the easier it is to generate a large permeation force and dynamic water pressure, which significantly impact the state of the soil [61]. It exerts an erosive force on loose cover layers, causing them to peel off and wash away, leading to

subsidence. By analyzing historical subsidence events, monitoring dates of groundwater levels, and geological drilling data, the difference between the maximum and minimum values of observed water levels from 2016 to 2022 is taken as the variation range of the groundwater level and is divided into four categories: >5 m, 3–5 m, 1–3 m, and <1 m (Figure 4f).

3.3. Evaluation of Susceptibility to Karst Ground Subsidence

We analyze the basic conditions for KGS separately, including the role and contribution of influencing factors under the basic conditions, and construct an impact judgment matrix based on their relative importance (Tables 2–5). The consistency ratio (CR) was used to evaluate the reliability of the constructed judgment matrix. A CR higher than 0.1 indicates an unreliable judgment requiring comparison and scoring modification. In this study, the CR calculated for simple sequences was 0.0, while that for total lines was 0.02; both values are lower than 0.1, indicating consistency between judgment matrices.

Table 2. Judgment matrix of factors to karst conditions.

Factors	Bedrock Lithology	Karst Development Degree	Weight Value
Bedrock lithology	1	1/3	0.2500
Karst development degree	3	1	0.7500

Table 3. Judgment matrix of factors to overburden conditions.

Factors	Bedrock Lithology	Lithology and Structure	Weight Value
Thickness	1	2	0.6667
Lithology and Structure	1/2	1	0.3333

Table 4. Judgment matrix of factors to hydrodynamic conditions.

Factors	Distance between Groundwater Level and Bedrock	Variation in Groundwater Level	Weight Value
Distance between groundwater level and bedrock	1	3	0.7500
Variation in groundwater level	1/3	1	0.2500

Table 5. Judgment matrix of condition layer to karst ground subsidence.

Indicators	Karst Conditions	Overburden Conditions	Hydrodynamic Conditions	Weight Value
Karst conditions	1	2	5	0.5813
Overburden conditions	1/2	1	3	0.3091
Hydrodynamic conditions	1/5	1/2	1	0.1096

The weights of basic conditions for KGS and influencing factors on these conditions can be obtained by normalization through calculating their maximum eigenvalues and corresponding eigenvectors (Table 6). The comprehensive evaluation model for susceptibility to KGS determines the contribution degree of influencing factors using a composite index method, as shown below.

The calculated comprehensive index divides the study area into extreme susceptibility, high susceptibility, medium susceptibility, and weak susceptibility using the natural segmentation method of the Geographic Information System (GIS). The results show the susceptibility zoning of KGS. We compared the results with existing subway lines and subway planning maps (2020–2035), combined with an analysis of land use types to analyze the triggering effect of human activities on KGS.

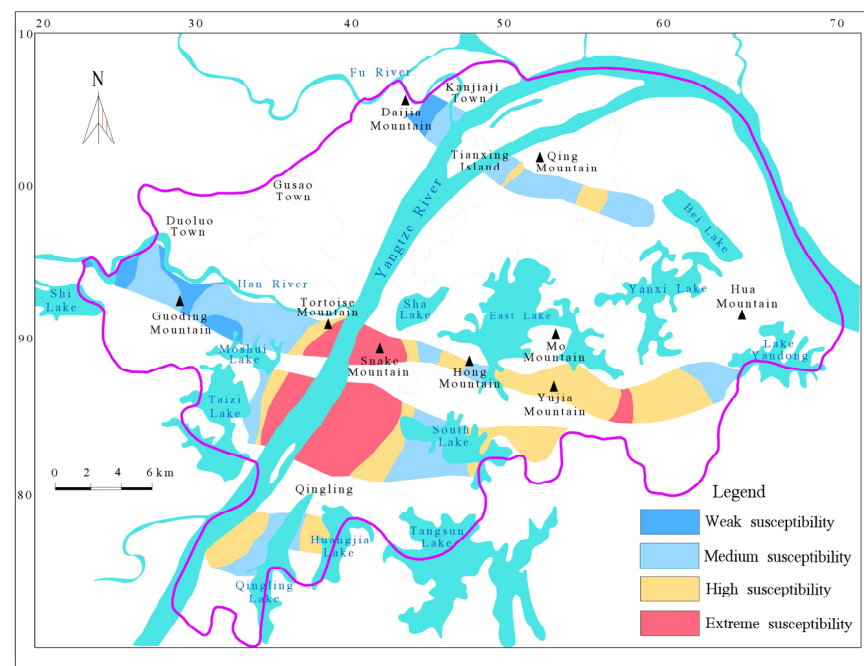
Table 6. Karst ground subsidence susceptibility assessment index weight table.

Indicator Layer	Weight Value	Factor Layer	Weight Value	Weight of Factor Unit
Karst condition	0.5813	Bedrock lithology	0.2500	0.146
		Karst development degree	0.7500	0.436
Overburden condition	0.3091	Thickness	0.6667	0.206
		Lithology and Structure	0.3333	0.103
Hydrodynamic conditions	0.1096	Distance between groundwater level and bedrock	0.7500	0.082
		Variation in groundwater level	0.2500	0.027

4. Discussion

4.1. KGS Susceptibility

The area of karst distribution in the study area is 155 km², with extreme susceptibility, high susceptibility, medium susceptibility, and weak susceptibility covering 7.64 km², 23.72 km², 51.48 km², and 72.16 km², accounting for 4.93%, 15.30%, 33.21%, and 46.56% of the total karst area, respectively (Figure 5).

**Figure 5.** Susceptibility zoning of karst ground subsidence in the study area.

The extreme-susceptibility areas are mainly distributed in Qingling Town, Snake Mountain, on the first terrace of the Yangtze River's southern carbonate belt. The bedrock lithology in this area is C-P limestone with a fault through it. The rock is broken and has karst fissures and caves. The overburden layer is relatively thick, with a thickness greater than 20 m, consisting of a binary structure of single-layer sand or thin clay layers. The groundwater level is close to the bedrock, less than 15 m. The geological conditions within the area are prone to induce ground subsidence due to karst erosion; many incidents have occurred historically. This indicates that the evaluation method used in this study for determining susceptibility levels aligns well with actual conditions and produces ideal results.

The sporadic distribution of the potential sinkhole-prone areas in high-susceptibility areas is located in Tortoise Mountain and the Yujia Mountain–Yanxi Lake regions. The bedrock lithology in this area is mainly Carboniferous limestone, with two faults developed within the region. The karst development degree near the Yangtze River area is relatively

strong. The thickness of the overburden layer is generally less than 20 m, while it is relatively thicker around Qingling Lake. Near the Yangtze River area, the structure of the overburden layer presents a binary structure with thin clay layers; while far away from the river area, most of them are single clay layers. The groundwater level is close to bedrock and has a close hydraulic connection with water sources such as Yangtze River water, pore water, and karst water.

Medium-susceptibility areas are mainly concentrated in the northern carbonate rock belt. The bedrock in this area is primarily composed of C limestone in the north of the belt, with weakly developed dissolution fissures, while S and K-E clastic rocks are dominant in the middle and southern belts, where there is no karst development. The thickness of the overburden layer is mostly greater than 30 m. The structure of the cover layer is a binary structure with a relatively large thickness of sticky sand or a single clay layer.

The weak-susceptibility areas mainly consist of coverage-type carbonate belts located far from the river. The bedrock in this area is composed of Silurian, Permian, and Devonian strata, with limited karst development. The thickness of the overburden layer is generally greater than 30 m. The groundwater level is approximately 30–45 m below the bedrock. There is a weak aquitard between the confined aquifer and the carbonate rock aquifer, which typically prevents karst subsidence from occurring.

4.2. Impact of Engineering Activities

Human activities are closely related to the susceptibility of KGS in the research area. Different types of human activities can induce varying degrees of KGS in different regions. Human engineering activities significantly trigger KGS [28,62].

According to the analysis of factors induced by human activities (Figure 6), it can be seen that the ground subsidence in karst areas mainly occurs in regions with more human activities, such as construction sites. Human activities, including the extraction of karst groundwater during construction, excavation pits, and the additional load from large buildings and warehouses, significantly impact the karst geo-environment. When the karst geological environment is fragile, KGS has a strong tendency to occur [6]. Some high-susceptibility areas and areas with weak susceptibility refer to regions with relatively stable geo-environmental conditions. These areas are characterized by more intensive human activities and engineering constructions. If the level of human activity in this area exceeds the stability of the karst geo-environment, there will be even more ground subsidence than in extreme-susceptibility areas [63]. There have been no occurrences of ground subsidence in some extreme-susceptibility areas. The reason is that these areas have lower human activity intensity and are mainly used for ecological and agricultural purposes without large-scale engineering construction. As a result, they have a minimal impact on the karst geological environment and are less likely to trigger ground subsidence caused by karst formations [14,57].

Combining the construction and planning maps of Wuhan's subway lines (Figure 7), it can be concluded that karst subsidence incidents have occurred near the subway lines, closely related to urban development. The construction or planning of subway lines can promote the appreciation of surrounding land values, thereby driving many engineering activities such as old city renovation around the line [64]. At the same time, the construction of subway lines and stations has led to extensive development and utilization of underground space. In these construction projects mentioned above, pile foundation compaction increases the load, leading to karst subsidence [49,65]. On the other hand, the excavation of foundation pits requires the pumping of groundwater, resulting in a significant variation in the water level and causing instability in the structure of overburdened sediment [22,42,58]. On a regional scale, these construction projects directly increase the susceptibility of KGS, resulting in the formation of sinkholes in shallow soil layers or below the bedrock limit, leading to cracking or collapsing surface buildings and infrastructure. And, like most geological hazards, the prevention and control of KGS should prioritize avoidance. Therefore, KGS imposes significant constraints on urban land development.

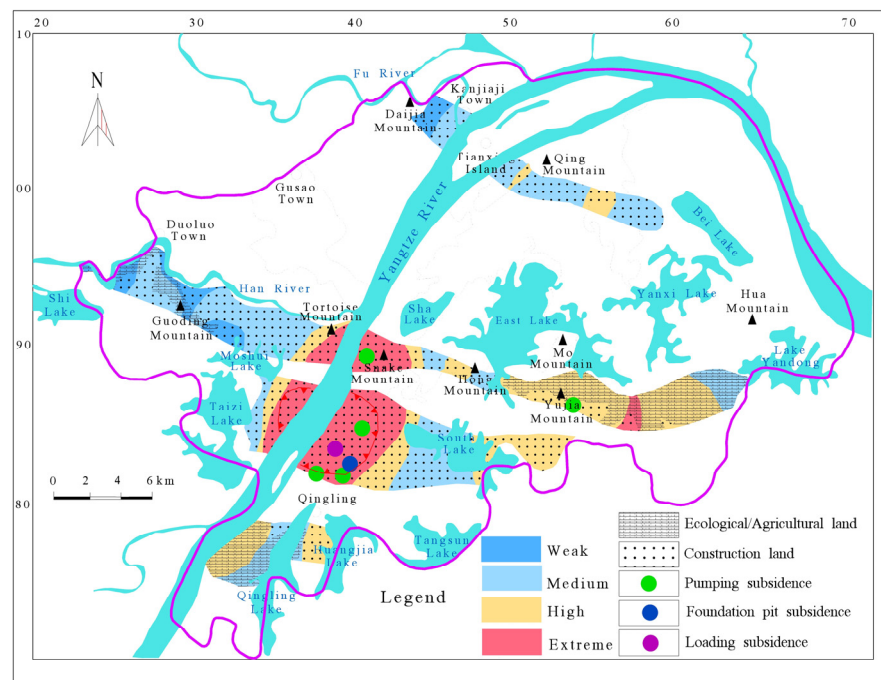


Figure 6. Human activity analysis map.

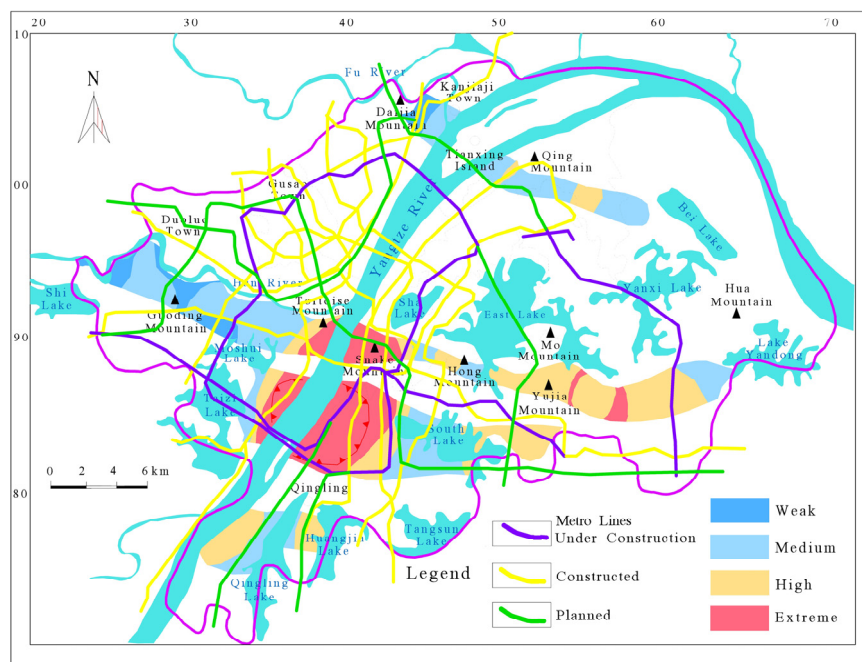


Figure 7. Subway line analysis map.

4.3. Suggestions for Partition Control

As an essential means to achieve a rational allocation of land resources, overall land use planning can adjust the structure and layout of land use at the macro level. Based on the analysis of KGS susceptibility evaluation and human activity characteristics, combined with the existing land use structure and layout, this study proposes a zoning control for subsequent land development. It puts forward prevention and control measures for KGS under different working conditions. Therefore, it is of practical significance to propose control suggestions for high-density urban core area land use planning.

Due to the binary structure of a single sand or clay covering in extreme-susceptibility areas, the sand layer causes the direct contact of soluble rocks with developed cracks and caves. When engineering construction in the area pumps groundwater, causing fluctuations in water levels, sand particles will become unstable under gravity or impact and leak into karst fissures or caves, ultimately inducing instability and rock subsidence of the covering layer [66]. In this case, when constructing a subway in extreme-susceptibility areas, it is necessary to consider adopting prevention and control technology measures, such as changing underground tunnels into elevated structures on the ground, effectively reducing or avoiding the harm of KGS [67]. When conducting engineering construction, preventing sand particle leakage should be prioritized by limiting pumping water quantity and slowing down fluctuations in the groundwater level [68]. For excavation during foundation pit earthwork excavation, using small excavators for gradual digging can reduce load-bearing pressure on lower rock–soil masses. To address increased regional loads due to strong compaction, increasing the density of sandy soil cover layers while lowering compressibility can prevent sand particle leakage and improve the anti-subsidence ability of soil layers. At the same time, dynamic compaction fills the lava fissures or caves directly beneath the covering layer of sandy soil, eliminating potential hazards. Based on the above, when extreme-susceptibility areas are planned for construction land, there are difficulties in development, large investments in engineering technology, and prominent safety hazards. Therefore, when planning land use, priority should be given to designating the extreme-susceptibility areas in the main urban area as land use types with lower engineering construction intensity, such as ecological land, to avoid their development and utilization as construction land [69]. Suppose the current land use in extreme-susceptibility areas is mainly low-rise residential neighborhoods with low development intensity during the urban renewal. In that case, it is advisable to maintain the existing land use intensity and avoid demolishing and constructing high-rise residential buildings. This will help ensure the stability of the regional geo-environmental carrying capacity.

The thickness of the covering layer in the high-susceptibility areas is generally less than 20 m, and the covering layer in the area around Qingling Lake is relatively thick. The structure of the overburden layer can be divided into two types: a binary structure with a thin clay layer near the Yangtze River region and mostly a single clay layer away from it; the distance between the groundwater level and bedrock is close, and there is a close hydraulic connection among the Yangtze River water, pore water, and karst groundwater. The degree of karst development in the lower part near the Yangtze River region is more substantial. Under seepage erosion, vacuum suction erosion, and engineering activities, the soil below the bottom of the overburden layer will be eroded to form soil caves, possibly leading to instability. In preventing and controlling KGS in high-susceptibility areas, the formation of soil caves in the overburden layer should be given priority. This can be achieved by replacing and filling voids with soil or grouting, eliminating vacuum pressure inside the caves, and controlling groundwater erosion and surface loads. When carrying out engineering construction, the pumping volume, water level drawdown, and well spacing should be limited to avoid excessive pumping from densely clustered wells. Properly place filter pipes in the developed areas of karst caves and the damaged sections of fault zones to prevent potential erosion caused by pumping water. If soil caves are formed above bedrock surfaces, they can be filled using compacted replacement or grouting methods until they disappear entirely. When the overburdened layer of soil is a binary structure with a clay layer beneath the sandy soil, it is necessary to protect the integrity of the clay layer during construction. If it is required to penetrate the barrier layer, effective measures should be taken to prevent sand fluid from leaking into the underlying cavities along exploration sites. Based on the above, high-susceptibility areas should prioritize maintaining the existing intensity of land use and preserving regional geological and environmental stability [70]. Before regional development and construction, a comprehensive evaluation of the geological and ecological carrying capacity should be conducted to ensure that human activities such as

regional building density and underground space development are limited to acceptable limits [71].

The land in the medium- and weak-susceptibility regions not prone to geological hazards is designated for engineering and construction purposes (industrial and residential land). The geological conditions of these sites are favorable, providing a solid foundation for construction projects. Under natural conditions, there is little risk of KGS. However, economic development needs and large-scale underground construction activities, such as groundwater extraction during the process, may affect the foundation's stability within a certain range. Therefore, it is necessary to strengthen management during engineering activities by reasonably arranging well clusters and strictly prohibiting excessive mining practices while implementing monitoring measures.

5. Conclusions

This study evaluates the susceptibility of KGS based on the analysis factors of karst development distribution, starting from regional geological and environmental conditions. The evaluation is conducted using the AHP-comprehensive index method. Furthermore, control measures for different susceptibility areas of human activities are proposed. The above analysis and control measures can provide a reference for other regions with comprehensive karst areas and rapidly developing cities such as Shenzhen and provide a basis for preventing ground collapse in areas with large-scale underground construction and urban renovation projects. However, the limitation of this study lies in the need for further strengthening targeted control measures and using more refined data to determine areas prone to KGS. For the unevenness of the vertical geological structure in karst areas, combining remote sensing image data or sensing gravity data can facilitate the identification of karst development regions [29,72]. Furthermore, machine learning can create detailed geological models using the measured data from hydrogeological and urban geological surveys as basic information [23,66,73]. This approach can reduce ground drilling and establish more accurate three-dimensional urban environmental and geological structure models. On the other hand, considering the impact of human activities on KGS, it is possible to construct quantitative models based on data such as building and road density to characterize the intensity of human activity. This approach allows us to utilize historical survey data to assess the impact of human activity at different stages of subway line planning, construction, and completion. Furthermore, it is possible to quantitatively analyze the effects of human activities on regional, geological, and environmental stability and regional KGS.

Author Contributions: Conceptualization and design, Lin Gao, Chuanming Ma; methodology, acquisition, and analysis of data, Lin Gao, Yan Shi; validation, Yang Qiu, Lin Gao; writing—original draft preparation, Lin Gao; funding acquisition, Aiguo Zhou, Chuanming Ma. All authors have read and agreed to the published version of the manuscript.

Funding: This study was supported by the Fundamental Research Funds for the Central Universities, China University of Geosciences (Wuhan) (No: CUGCJ1822).

Data Availability Statement: The authors do not have permission to share data.

Acknowledgments: The authors thank Qian Jing and Fu Xiaomin for modifying the language structure.

Conflicts of Interest: The authors declare no conflict of interest. The funders had no role in the study's design; in the collection and analyses of data; in the writing of the manuscript; or in the decision to publish the results.

References

1. Parise, M. Karst Geo-Hazards: Causal Factors and Management Issues Naravne Nesreče Na Krasu: Vzročni Dejavniki in Vprašanja Upravljanja. *Acta Carsologica* **2015**, *3*, 44.
2. Chen, Z.; Auler, A.S.; Bakalowicz, M.; Drew, D.; Griger, F.; Hartmann, J.; Jiang, G.; Moosdorf, N.; Richts, A.; Stevanovic, Z.; et al. The World Karst Aquifer Mapping Project: Concept, Mapping Procedure and Map of Europe. *Hydrogeol. J.* **2017**, *25*, 771–785. [[CrossRef](#)]

3. Goldscheider, N.; Chen, Z.; Auler, A.S.; Bakalowicz, M.; Broda, S.; Drew, D.; Hartmann, J.; Jiang, G.; Moosdorf, N.; Stevanovic, Z.; et al. Global Distribution of Carbonate Rocks and Karst Water Resources. *Hydrogeol. J.* **2020**, *28*, 1661–1677. [[CrossRef](#)]
4. Murck, B.W.; Skinner, B.J.; Porter, S.C. *Encyclopedia of Sustainability Science and Technology Series*; Springer: Berlin/Heidelberg, Germany, 1996; Volume i, ISBN 0471303569.
5. Jiang, Z.; Lian, Y.; Qin, X. Rocky Desertification in Southwest China: Impacts, Causes, and Restoration. *Earth-Sci. Rev.* **2014**, *132*, 1–12. [[CrossRef](#)]
6. Tolmachev, V.V.; Neshchetkin, O.B. Evaluation of Karst Hazards for Civil and Industrial Buildings. *Acta Geol. Sin.-Engl. Ed.* **2010**, *75*, 269–274. [[CrossRef](#)]
7. Ford, D.; Williams, P. *Karst Hydrogeology and Geomorphology*; Wiley: Hoboken, NJ, USA, 2013; ISBN 9781118684986.
8. Perrin, J.; Cartannaz, C.; Noury, G.; Vanoudheusden, E. A Multicriteria Approach to Karst Subsidence Hazard Mapping Supported by Weights-of-Evidence Analysis. *Eng. Geol.* **2015**, *197*, 296–305. [[CrossRef](#)]
9. Bees, A.H.; Mites, B. Water-Formed Structures Geothermometry. *Science* **1988**, *243*, 1618–1619.
10. Siska, P.P.; Goovaerts, P.; Hung, I.K. Evaluating Susceptibility of Karst Dolines (Sinkholes) for Collapse in Sango, Tennessee, USA. *Prog. Phys. Geogr.* **2016**, *40*, 579–597. [[CrossRef](#)]
11. YongYao, W.; ShuLin, S. Comprehensive Critical Mechanical Model of Covered Karst Collapse under the Effects of Positive and Negative Pressure. *Bull. Eng. Geol. Environ.* **2018**, *77*, 177–190. [[CrossRef](#)]
12. Kaufmann, O.; Quinif, Y. Geohazard Map of Cover-Collapse Sinkholes in the “Tournaisis” Area, Southern Belgium. *Eng. Geol.* **2002**, *65*, 117–124. [[CrossRef](#)]
13. Zhao, W.; Gan, F.; Meng, Y.; Zheng, Z.; Liu, X. Application of Seismic Velocity Tomography in Investigation of Karst Collapse Hazards, Guangzhou, China. *Environ. Earth Sci.* **2018**, *77*, 258. [[CrossRef](#)]
14. Vierrether, C.B. Urban Development in Karst and Collapse-Prone Geologic Environments. *Carbonates Evaporites* **2013**, *28*, 23–29. [[CrossRef](#)]
15. Yilmaz, I.; Marschalko, M.; Bednarik, M. An Assessment on the Use of Bivariate, Multivariate and Soft Computing Techniques for Collapse Susceptibility in GIS Environ. *J. Earth Syst. Sci.* **2013**, *122*, 371–388. [[CrossRef](#)]
16. Martínez-Moreno, F.J.; Galindo-Zaldívar, J.; González-Castillo, L.; Azañón, J.M. Collapse Susceptibility Map in Abandoned Mining Areas by Microgravity Survey: A Case Study in Candado Hill (Málaga, Southern Spain). *J. Appl. Geophys.* **2016**, *130*, 101–109. [[CrossRef](#)]
17. Zhong, R.; He, D.; Hu, J.; Duan, X.; Huang, J.; Cheng, X. Distribution and Susceptibility Assessment of Collapses and Landslides in the Riparian Zone of the Xiaowan Reservoir. *Chin. Geogr. Sci.* **2019**, *29*, 70–85. [[CrossRef](#)]
18. Ma, C.-X.; Peng, F.-L. Monetary Evaluation Method of Comprehensive Benefits of Complex Underground Roads for Motor Vehicles Orienting Urban Sustainable Development. *Sustain. Cities Soc.* **2021**, *65*, 102569. [[CrossRef](#)]
19. Maltsev, A.; Baranova, M.; Ponomarenko, A. Buildings and Constructions Safety Operation on Karstic Territories of the Samara City. *MATEC Web Conf.* **2017**, *106*, 02029. [[CrossRef](#)]
20. Pueyo Anchuela, O.; Casas Sainz, A.M.; Pocoví Juan, A.; Gil Garbí, H. Assessing Karst Hazards in Urbanized Areas. Case Study and Methodological Considerations in the Mantle Karst from Zaragoza City (NE Spain). *Eng. Geol.* **2015**, *184*, 29–42. [[CrossRef](#)]
21. Dos Santos, E.S.M.; Silva, R.W.S.; Sampaio, E.E.S. Analysis of the Risk of Karst Collapse in Lapão, Bahia, Brazil. *Explor. Geophys.* **2012**, *43*, 198–212. [[CrossRef](#)]
22. Li, X.; Zhou, S.; Xu, G. GIS-Based Risk Assessment to Karst Susceptibility of Shenzhen Universiade Center (China). *Procedia Environ. Sci.* **2011**, *10*, 1389–1395. [[CrossRef](#)]
23. Hu, J.; Motagh, M.; Wang, J.; Qin, F.; Zhang, J.; Wu, W.; Han, Y. Karst Collapse Risk Zonation and Evaluation in Wuhan, China Based on Analytic Hierarchy Process, Logistic Regression, and Insar Angular Distortion Approaches. *Remote Sens.* **2021**, *13*, 5063. [[CrossRef](#)]
24. Papadopoulou-Vrynioti, K.; Bathrellos, G.D.; Skilodimou, H.D.; Kaviris, G.; Makropoulos, K. Karst Collapse Susceptibility Mapping Considering Peak Ground Acceleration in a Rapidly Growing Urban Area. *Eng. Geol.* **2013**, *158*, 77–88. [[CrossRef](#)]
25. Xiong, X.; Zhou, T.; Cai, T.; Huang, W.; Li, J.; Cui, X.; Li, F. Land Use Transition and Effects on Ecosystem Services in Water-Rich Cities under Rapid Urbanization: A Case Study of Wuhan City, China. *Land* **2022**, *11*, 1153. [[CrossRef](#)]
26. Liu, S.-C.; Peng, F.-L.; Qiao, Y.-K.; Zhang, J.-B. Evaluating Disaster Prevention Benefits of Underground Space from the Perspective of Urban Resilience. *Int. J. Disaster Risk Reduct.* **2021**, *58*, 102206. [[CrossRef](#)]
27. Hao, J.; Lin, Q.; Wu, T.; Chen, J.; Li, W.; Wu, X.; Hu, G.; La, Y. Spatial–Temporal and Driving Factors of Land Use/Cover Change in Mongolia from 1990 to 2021. *Remote Sens.* **2023**, *15*, 1813. [[CrossRef](#)]
28. Tan, R.; Liu, Y.; Liu, Y.; He, Q.; Ming, L.; Tang, S. Urban Growth and Its Determinants across the Wuhan Urban Agglomeration, Central China. *Habitat Int.* **2014**, *44*, 268–281. [[CrossRef](#)]
29. Lai, W.; Shen, Q.; Wang, H.; Shum, C.K.; Jiang, L.; Yang, B.; Dong, J.; Gao, F.; Zhao, Y.; Liu, T. InSAR-Derived Land Subsidence in Wuhan between 2015 and 2020. *All Earth* **2022**, *34*, 224–242. [[CrossRef](#)]
30. Greater London Authority. 2021. Available online: <https://Data.London.Gov.Uk/> (accessed on 19 September 2022).
31. United States Census Bureaus. 2021. Available online: www.census.gov (accessed on 19 September 2022).
32. Statistical Office of the Prime Minister’s Office of Japan. 2021. Available online: www.e-stat.go.jp (accessed on 19 September 2022).
33. Hu, X.; Gao, L.; Ma, C.; Hu, X. Land Use Zoning of Weifang North Plain Based on Ecological Function and Geo-Environmental Suitability. *Bull. Eng. Geol. Environ.* **2020**, *79*, 2697–2719. [[CrossRef](#)]

34. Chen, J.; MA, I. Urban Growth Pattern Modelling: A Case Study of Wuhan City, PR China. *Landsc. Urban Plan.* **2015**, *62*, 199–217. [[CrossRef](#)]
35. Qiu, Y.; Zhou, A.; Li, M.; Guo, Y.; Cui, H.; Ma, C. Territorial Spatial Usage Regulation Based on Resources Endowment and Sustainable Development: A Case of Wuhan, China. *J. Clean. Prod.* **2023**, *385*, 135771. [[CrossRef](#)]
36. Guo, Z.; Guo, H. The Impact of Metro Construction on Regional Economy—Wuhan as an Example. *Financ. Econ.* **2014**, *2*, 86–87. (In Chinese) [[CrossRef](#)]
37. Zheng, S.; Hu, X.; Wang, J.; Wang, R. Subways near the Subway: Rail Transit and Neighborhood Catering Businesses in Beijing. *Transp. Policy* **2016**, *51*, 81–92. [[CrossRef](#)]
38. Ting, Y. *The Research of the Post Evaluation of Socio-Economic Impacts on Tianjin Subway Construction Project*; Hebei University of Technology: Tianjin, China, 2014.
39. Du, N.; Ottens, H.; Sliuzas, R. Spatial Impact of Urban Expansion on Surface Water Bodies—A Case Study of Wuhan, China. *Landsc. Urban Plan.* **2010**, *94*, 175–185. [[CrossRef](#)]
40. Li, G.; Sun, S.; Fang, C. The Varying Driving Forces of Urban Expansion in China: Insights from a Spatial-Temporal Analysis. *Landsc. Urban Plan.* **2018**, *174*, 63–77. [[CrossRef](#)]
41. Song, Y.; Yeung, G.; Zhu, D.; Xu, Y.; Zhang, L. Efficiency of Urban Land Use in China’s Resource-Based Cities, 2000–2018. *Land Use Policy* **2022**, *115*, 106009. [[CrossRef](#)]
42. Li, X.; Yin, K.; Chen, B.; Li, Y.; Chao, J.; Li, J. Evaluation of Susceptibility to Karst Collapse on Both Sides of the Yangtze River in Baishazhou, Wuhan and Preventive Measures in the Process of Metro Construction. *Bull. Geol. Sci. Technol.* **2020**, *39*, 121–130. [[CrossRef](#)]
43. Bollinger, C.R.; Ihlanfeldt, K.R. The Impact of Rapid Rail Transit on Economic Development: The Case of Atlanta’s MARTA. *J. Urban Econ.* **1997**, *42*, 179–204. [[CrossRef](#)]
44. Adolphson, M.; Fröidh, O. Impact on Urban Form by the Localization of Railway Stations: Evidence from Sweden. *Cities* **2019**, *95*, 102362. [[CrossRef](#)]
45. Keqiang, H.; Changli, L.; Sijing, W. Karst Collapse Mechanism and Criterion for Its Stability. *Acta Geol. Sin.-Engl. Ed.* **2001**, *75*, 330–335. [[CrossRef](#)]
46. Liao, L.; Zhang, J.; Wu, K.; Yiping, G. Development Law and Risk Assessment of Karst Ground Collapse in the Third Ring Road Area of Wuhan, Hubei Province. *Chin. J. Geol. Hazard Control* **2018**, *29*, 78–86. (In Chinese) [[CrossRef](#)]
47. Hu, S.; Tong, L.; Frazier, A.E.; Liu, Y. Urban Boundary Extraction and Sprawl Analysis Using Landsat Images: A Case Study in Wuhan, China. *Habitat Int.* **2015**, *47*, 183–195. [[CrossRef](#)]
48. Li, Z.G.; Xiao, S.D.; Pan, Y.H.; Lu, S.W. The Hazard Assessment of Karst Surface Collapse Risk Zoning Based on BP Neural Network in Wuhan City. *Appl. Mech. Mater.* **2013**, *405–408*, 2376–2379. [[CrossRef](#)]
49. Wang, X.; Lai, J.; He, S.; Garnes, R.S.; Zhang, Y. Karst Geology and Mitigation Measures for Hazards during Metro System Construction in Wuhan, China. *Nat. Hazards* **2020**, *103*, 2905–2927. [[CrossRef](#)]
50. Yu, L.; Yu, T. Analysis of Collapse-Causing Model of Karst Collapse in Wuhan. *Resour. Environ. Eng.* **2015**, *29*, 887–891. (In Chinese)
51. Wu, Y.; Jiang, X.; Guan, Z.; Luo, W.; Wang, Y. AHP-Based Evaluation of the Karst Collapse Susceptibility in Tailai Basin, Shandong Province, China. *Environ. Earth Sci.* **2018**, *77*, 436. [[CrossRef](#)]
52. Dan, L. Comparison of Indicators for the Assessment of Saltwater Intrusion in Coastal Aquifers—Taking Aquifers in Pearl River Estuary as an Example. *Mar. Environ. Sci.* **2020**, *39*, 16–23. (In Chinese) [[CrossRef](#)]
53. Xiao, X.; Li, Z.; Cai, G.; Yang, H. Effects of Declining Water Levels on Water-Air Interactions in Cover Collapse Sinkhole. *Bull. Eng. Geol. Environ.* **2021**, *80*, 2545–2556. [[CrossRef](#)]
54. Saaty, T.L. The Modern Science of Multicriteria Decision Making and Its Practical Applications: The AHP/ANP Approach. *Oper. Res.* **2013**, *61*, 1101–1118. [[CrossRef](#)]
55. Saaty, T.L. Decision-Making with the AHP: Why Is the Principal Eigenvector Necessary. *Eur. J. Oper. Res.* **2003**, *145*, 85–91. [[CrossRef](#)]
56. Masuda, T. Hierarchical Sensitivity Analysis of Priority Used in Analytic Hierarchy Process. *Int. J. Syst. Sci.* **1990**, *21*, 415–427. [[CrossRef](#)]
57. Gao, L.; Hu, X.; Ma, C.; Kuang, H.; Qi, H.; He, Z. Geoenvironmental Risk Evaluation of High-Efficiency Eco-Economic Zone in Weifang City, China. *Nat. Hazards Rev.* **2020**, *21*, 05020005. [[CrossRef](#)]
58. Xu, G. *Mechanism and Hazard Assessment of Covered Karst Sinkholes in Wuhan City, China*; China University of Geosciences: Wuhan, China, 2016. (In Chinese)
59. Yu, J.; Zhu, Y.; Yao, W.; Liu, X.; Ren, C.; Cai, Y.; Tang, X. Stress Relaxation Behaviour of Marble under Cyclic Weak Disturbance and Confining Pressures. *Meas. J. Int. Meas. Confed.* **2021**, *182*, 109777. [[CrossRef](#)]
60. He, K.; Jia, Y.; Wang, B.; Wang, R.; Luo, H. Comprehensive Fuzzy Evaluation Model and Evaluation of the Karst Collapse Susceptibility in Zaozhuang Region, China. *Nat. Hazards* **2013**, *68*, 613–629. [[CrossRef](#)]
61. Chen, X.; Guo, R.; Tang, L.; Zhang, X. Study on Ground Collapse of Covered Karst Soil Caves by Sudden Drop of Groundwater. *Adv. Civ. Eng.* **2021**, *2021*, 7796401. [[CrossRef](#)]
62. Santo, A.; Budetta, P.; Forte, G.; Marino, E.; Pignalosa, A. Karst Collapse Susceptibility Assessment: A Case Study on the Amalfi Coast (Southern Italy). *Geomorphology* **2017**, *285*, 247–259. [[CrossRef](#)]

63. Liu, Y.; Luo, T.; Liu, Z.; Kong, X.; Li, J.; Tan, R. A Comparative Analysis of Urban and Rural Construction Land Use Change and Driving Forces: Implications for Urban-Rural Coordination Development in Wuhan, Central China. *Habitat Int.* **2015**, *47*, 113–125. [[CrossRef](#)]
64. Zhang, Y.; Xie, Z.; Jiang, F.; Xu, T.; Yang, S.; Yin, S.; Zhao, F.; He, J.; Chen, Y.; Hou, Z.; et al. Evaluating the Socioeconomic Value of Urban Underground Space in Kunming, China, Using the Entropy Method and Exponential Smoothing Prediction. *J. Urban Plan. Dev.* **2023**, *149*, 1–14. [[CrossRef](#)]
65. Chen, W.F.; Gong, H.L.; Chen, B.B.; Liu, K.S.; Gao, M.; Zhou, C.F. Spatiotemporal Evolution of Land Subsidence around a Subway Using InSAR Time-Series and the Entropy Method. *GIScience Remote Sens.* **2017**, *54*, 78–94. [[CrossRef](#)]
66. Pan, Z.; Chen, X.; Yang, X.; Song, Y.; Ban, R.; Zhang, M. Formation Mechanism Analysis of Cover Collapse Sinkholes in Wugaishan Town, Chenzhou City, Hunan Province, China. *Environ. Earth Sci.* **2022**, *81*, 48. [[CrossRef](#)]
67. Rodriguez, V.; Gutiérrez, F.; Green, A.G.; Carbonel, D.; Horstmeyer, H.; Schmelzbach, C. Characterizing Sagging and Collapse Sinkholes in a Mantled Karst by Means of Ground Penetrating Radar (GPR). *Environ. Eng. Geosci.* **2014**, *20*, 109–132. [[CrossRef](#)]
68. Mochales, T.; Pueyo, E.L.; Casas, A.M.; Soriano, M.A. Magnetic Prospection as an Efficient Tool for Doline Detection: A Case Study in the Central Ebro Basin (Northern Spain). *Geol. Soc. Spec. Publ.* **2007**, *279*, 73–84. [[CrossRef](#)]
69. Wei, S.; Luan, Q.; Huang, C.; Gu, X. Review and Prospects on Researches on Soft Measures of Land-Use Planning in Prevention and Control of Geological Disasters. *J. Nat. Disasters* **2014**, *23*, 159–165. [[CrossRef](#)]
70. Zacharias, J.; He, J. Hong Kong's Urban Planning Experiment in Enhancing Pedestrian Movement from Underground Space to the Surface. *Tunn. Undergr. Sp. Technol.* **2018**, *82*, 1–8. [[CrossRef](#)]
71. Panno, S.V.; Luman, D.E. Characterization of Cover-Collapse Sinkhole Morphology on a Groundwater Basin-Wide Scale Using Lidar Elevation Data: A New Conceptual Model for Sinkhole Evolution. *Geomorphology* **2018**, *318*, 1–17. [[CrossRef](#)]
72. Currens, J.C. Hypothesized Mechanism for the Initiation of Soil Cavities and Subsequent Cover-Collapse in Karst Terrain. *J. Cave Karst Stud.* **2018**, *80*, 172–180. [[CrossRef](#)]
73. Zheng, Q.; Zhao, P.; Li, Y.; Wang, H.; Yang, Y. Spectrum Interference-Based Two-Level Data Augmentation Method in Deep Learning for Automatic Modulation Classification. *Neural Comput. Appl.* **2021**, *33*, 7723–7745. [[CrossRef](#)]

Disclaimer/Publisher's Note: The statements, opinions and data contained in all publications are solely those of the individual author(s) and contributor(s) and not of MDPI and/or the editor(s). MDPI and/or the editor(s) disclaim responsibility for any injury to people or property resulting from any ideas, methods, instructions or products referred to in the content.